J. Pharm. Pharmacol. 1998, 50: 837–844
Received February 25, 1998
Accepted April 15, 1998

Solution-structure of a Peptide Designed to Mimic the C-terminal Hexapeptide of Endothelin

C. F. VAN DER WALLE, S. BANSAL AND D. J. BARLOW

Pharmacy Department, King's College, London SW3 6LX, UK

Abstract

The peptide: Ac-cyclo(Cys-His-Leu-Asp-Cys)-Ile-Trp-OH, has been designed by computer-aided molecular-modelling techniques to mimic the proposed α-helical conformation of the C-terminal hexapeptide of endothelin.

Two-dimensional proton nuclear magnetic resonance spectra were acquired for the peptide dissolved in d_6-DMSO or D_2O–H_2O and the distance and angle constraints incorporated into simulated annealing experiments. Conformers generated from the D_2O–H_2O data superposed on the corresponding main-chain atoms in the crystal structure of endothelin 1 and the solution structure of BQ-123 with root mean square co-ordinate differences of 0·9 Å and 0·77 Å, respectively. The peptide did not elicit antagonism of endothelin-induced in-vitro contractions of rabbit aorta (endothelin A receptor) or rabbit bronchus (endothelin B receptor) preparations.

Because the peptide can adopt a conformer which closely matches the equivalent residues in the endothelin 1 crystal structure and in BQ-123, we suggest BQ-123 does not necessarily mimic the endothelin C-terminal region to achieve its antagonism, and that a helical conformation of the endothelin C-terminal hexapeptide does not favour its interaction at the endothelin B receptor.

Endothelin is a potent vasoconstrictor peptide produced by the mammalian endothelium (Yanagisawa et al 1988). It is known to be involved in the pathology of pulmonary disease (Barnes 1994), in the development of craniofacial tissues (Kurihara et al 1994) and in cardiovascular and renal diseases (Newby & Webb 1996). Considerable attention has been focused on the development of endothelin antagonists, which could provide useful therapeutic agents. The cyclic peptide antagonist, BQ-123 (Ishikawa et al 1992) has already been shown to prevent early cerebral vasospasm after haemorrhage (Clozel & Watenabe 1993) and to protect against ischaemic acute renal failure in rats (Mino et al 1992). The rational design of small-peptide antagonists has been largely focused on the endothelin C-terminal hexapeptide which has been shown to be a full agonist at the endothelin B receptor but not the endothelin A receptor (Maggi et al 1989). Amino-acid substitution and modification of the hexapeptide has led to the discovery of many non-selective endothelin receptor peptide antagonists, in turn providing clues to some of the structural determinants of endothelin-receptor recognition (Cody et al 1995). Further design of selective antagonists would be greatly aided by detailed information about the 3-dimensional structure of this binding pocket, which remains uncharacterized.

Many structural data for the endothelin peptide have, however, been obtained from circular dichroism (CD) (Perkins et al 1990), proton nuclear magnetic resonance (^{1}H NMR) (Saudek et al 1991; Coles et al 1993), X-ray crystallography (Janes et al 1994) and fluorescence experiments (Pelton 1991). ^{1}H NMR studies of endothelin have consistently shown that the region spanning Lys^9 to Cys^{15} has an α-helical conformation; the C-terminal hexapeptide tail region is much less well defined (Mills et al 1992). A plausible structure for this region was found by X-ray crystallography which showed that the α-helix in the molecule extended from Lys^9 down to Trp^{21} (Janes et al 1994). Although it has been suggested that the crystal structure of endothelin represents the biologically relevant conformer of endothelin (Wallace & Janes 1995), there is no direct evidence to support this view. In this

Correspondence: D. J. Barlow, Pharmacy Department, King's College London, London SW3 6LX, UK.

study we have used the X-ray crystal structure of endothelin as reference and have attempted to determine the 3-D structure and activity of a small peptide designed to mimic the α-helical C-terminal hexapeptide. The amino acid sequence of the peptide was conserved as found for endothelin residues 15 to 21, but with an Ile^{19} to Cys substitution to enable cyclization via a disulphide, to approximate an α-helical turn. By modelling the peptide's conformation in solution using data derived from two-dimensional (2-D) ^{1}H NMR studies (complemented by CD experiments) it was hoped that we could validate the original design and correlate the observed structure of the peptide with its pharmacological activity.

Materials and Methods

Materials

Endothelin 1 and L amino acids were purchased from Calbiochem-Novabiochem (UK) Ltd. Carbachol, noradrenaline, d_6-DMSO, D_2O (99·9 atom-percent D), sodium lauryl sulphate, trifluoroethanol, hydrochloric acid and sodium hydroxide were obtained from Aldrich (UK).

Peptide synthesis

The Fmoc solid-phase synthesis of the peptide was performed as described previously (Van der Walle et al 1996)—loading on to PEG-polystyrene resin with a trityl linker, in-situ coupling of the amino acids, and protection of the side-chains of His and Cys with the trityl group and that of Asp by *t*-Butyl. After cleavage from the resin with tri-isopropylsilane–phenol–water–trifluoroacetic acid (1 : 5 : 5 : 89) the crude peptide was purified by reverse-phase high-performance liquid chromatography and characterized by fast-atom bombardment mass spectrometry and capillary zone electrophoresis.

^{1}H NMR spectroscopy

1-D and 2-D ^{1}H NMR spectra of the cyclic peptide were recorded by means of a 400 MHz Bruker AMX spectrometer equipped with an Aspect 3000 workstation. The peptide samples were prepared at concentrations of 3 mM and no adjustment of pH was made to the samples in D_2O–H_2O. All spectra were recorded at 25°C and referred either to the DMSO residual proton signal at 2·50 ppm (for spectra recorded with the sample dissolved in d_6-DMSO) or to the water resonance at 4·80 ppm (for spectra recorded with the sample dissolved in D_2O–H_2O or D_2O). 1-D spectra were recorded with a sweep-width of 8064 Hz and had a resolution of 0·49 Hz point-1. 2-D proton–proton shift-correlated spectroscopy (COSY) experiments were performed using either COSY90 or COSY45, or using double quantum-filtering (COSYDQF). Nuclear Overhauser effect spectroscopy (NOESY) spectra were acquired with mixing times (τ_m) of 150, 300 or 450 ms in d_6-DMSO and 50, 100, 200 or 300 ms in H_2O–D_2O for examination of proton–proton dipolar couplings through NOE build-up. Suppression of the water signal arising from the D_2O–H_2O samples was achieved by continuous low-power irradiation during the relaxation delay and for the NOESY experiments during the mixing time also. Spectra acquired in the phase-sensitive mode (COSYDQF and NOESY) were processed according to the time proportional phase incrementation method (Marrion & Wüthrich 1983) using a squared sine-wave function.

Peaks were assigned sequentially using the method of Wüthrich (1986) and the cross-peak volumes were obtained by integration using the program Aurelia (Bruker software). NOE distance constraints were determined using the cross-peak volumes, calibrated with reference to the integral observed for the cross-peak for the Trp *ortho*-aromatic hydrogens, $H\zeta^3/H\varepsilon^3$ and $H\zeta^2/H\eta^2$, taken to be 2·5 Å apart. The NOEs were accordingly classified as strong, medium or weak with the corresponding inter-proton distance limits set to 2·0, 3·0 and 4·0 Å for d_6-DMSO data, and 2·0, 2·5 and 3·8 Å for the D_2O–H_2O data. All methylene and methyl protons involved in the definition of an NOE were approximated using the associated carbon atom to represent their mid-point using a correction factor of 1·0 Å added to the corresponding distance boundaries. ϕ torsion angles were calculated from the NH resonance in ^{1}H NMR spectra using the Karplus equation (Sutcliffe 1993). χ_1 torsion angles were calculated by use of the $^{\alpha\beta}J_{Hz}$ values and the relative strengths of the $d_{\beta N}$ NOE cross-peaks (Barsukov & Lian 1993).

Circular dichroism

Circular dichroism spectra of the peptide samples were recorded with Jasco J-740 and J-600 spectropolarimeters and the UV profiles were recorded with an AVIV 17DS spectrophotometer. For pH titration experiments the peptide was dissolved in H_2O at a concentration of 192 $\mu g\,mL^{-1}$ and the pH adjusted over the range pH 2·4–11·3 by use of HCl(aq) and NaOH(aq); measurements were made with a pH PocketFET (Sentron). Peptide samples were also prepared in saturated sodium lauryl sulphate solution and trifluoroethanol at the same concentration. CD and UV measurements were made over the peptide (180–260 nm) and disulphide-aromatic (230–360 nm) regions in superseal

quartz cells (Hellma) with path lengths 0·05 and 1·0 cm, respectively.

Molecular modelling

All molecular modelling work was performed on a Silicon Graphics Iris 4D/35 TG workstation. In-vacuo molecular mechanics and molecular dynamics (MD) calculations were performed using Hyperchem (Hypercube). Molecular potential energies were calculated by use of the Amber force-field (Weiner et al 1986) and energy minimizations achieved over 300 iterations by use of the Polak-Ribiere algorithm. Cluster analyses of the peptide conformers were performed according to methods described by Perkins & Barlow (1990), and the molecular superpositions obtained and quantified by the method of McLachlan using the Matfit routine (McLachlan 1979).

For the simulated annealing experiments incorporating the NMR data, starting conformers were generated using the program Ramble (Perkins & Barlow 1990). The relevant side-chains and disulphide bridge were then added manually and the resulting conformers energy-minimized to eliminate unfavourable non-bonded interactions. Structures were then heated to 750 K and sampled every 1 ps over an MD period of 15 ps at 750 K. During this period peptide bonds were constrained to *trans* and the chirality of the residues maintained via an improper torsion angle. Experimentally determined distance and torsion-angle constraints, calculated from the above NMR data, were applied with force constants similar to the default values of the Amber force field. The van der Waals scale factor was reduced to 0·0002 and electrostatic forces were ignored to enable better conformational sampling. The sampled structures were cooled in 25-K stages to 300 K during which time the van der Waals scale factor was increased to 1·0 and the force constants of all the applied constraints reduced towards zero. Energy minimizations of the cooled structures were performed in the absence of distance and torsion angle constraints.

The resulting peptide conformers were analysed using a suite of in-house programs to check for violations of the experimental distance and torsion angle constraints and to ensure that all main-chain torsion angles were sensible. In addition back-calculations of theoretical NOEs between main-chain atoms were calculated to monitor for NOEs not seen experimentally. The final sets of conformers selected were chosen so that all ϕ angles fell in the allowed ranges, the majority of violations were less than 1·0 Å and no unobserved NOE contacts were present.

Pharmacology

Male New Zealand white rabbits, 2–2·5 kg, were killed by intravenous injection of pentobarbitone sodium (60 mg kg^{-1}) and the descending thoracic aorta and upper bronchi excised and trimmed of connective tissue and fat. The aortal endothelium was removed by rolling a plastic tube inside the lumen of the aorta. Antagonist studies involved 30 min preincubation of the peptide (15 μM bath concentration) before cumulative addition of endothelin, with 5-mm ring segments of either the aorta or bronchi mounted in a 20-mL organ bath with freshly prepared Krebs-Henseleit buffer solution maintained at 37°C and oxygenated with O_2–CO_2 (95% : 5%). The aortal and bronchal ring preparations were left to equilibrate for 60 min under 1 g and 1·5 g tension, respectively. Agonist studies involving cumulative additions of the peptide were performed in 2·5-mL organ baths with aortal ring segments equilibrated as above.

The integrity of the aortal and bronchal preparations was checked by monitoring their responses to 10 μM noradrenaline and 10 μM acetylcholine, respectively. Responses to endothelin, subsequent to incubation with the test peptide, were expressed as a percentage of the half-maximum response to endothelin in the control. Effectiveness of the removal of aortal endothelium was tested by checking for the absence of relaxation in response to 10 μM carbachol before noradrenaline wash out.

Results

NMR experiments

By use of the COSY and NOESY spectra for the peptide dissolved in d_6-DMSO and D_2O–H_2O, all proton signals were assigned with the exception of those for the His βCH in d_6-DMSO and the His and Trp αCH in D_2O–H_2O (Table 1). The chemical shifts for protons in the side-chains of Leu^3, Ile^6, Trp^7 and His^2 were readily assigned on the basis of their typical spin systems, and the Ile^6 and Leu^3 αCH signals were then assigned by tracing the connectivities to their corresponding βCH. In both experiments the Cys^1 NH was readily identified by its strong NOE cross-peak to the acetate methyl protons and this led to the assignment of the Cys^1 αCH and His^2 NH and so on in a sequential manner.

NOE build-up was followed over increasing τ_m, with the identification of long-range NOEs at 100 ms. In both solvents some of the long-range NOEs found were later disregarded because of ambiguities arising from the degenerate nature of the signals for the Ile^6 and Leu^3 NH, and Leu^3 and His^2 βCH in d_6-DMSO, and Trp^7 and Leu^3 NH in

Table 1. Proton resonance assignments (ppm) for the cyclic peptide as observed in the nuclear Overhauser effect spectroscopy experiment in D_2O-H_2O.

Residue	NH	αCH	βCH	Other	
Ac				CH_3	2·02
Cys^1	8·40	4·44	3·00		
			3·19		
His^2	9·17	*	3·20	δ^2CH	7·36
			3·38	ε^1CH	8·67
Leu^3	8·22	4·50	1·67	γCH	1·40
			1·67	δCH_3	0·92
					0·97
Asp^4	8·91	4·56	2·89		
			3·08		
Cys^5	8·18	4·48	2·60		
			2·94		
Ile^6	8·13	4·14	1·80	γCH	1·10
					1·37
				γCH_3	0·84
				δCH_3	0·82
Trp^7	8·22	*	3·41	δ^1CH	7·27
			3·24	ε^1CH	10·13
				ε^3CH	7·71
				ζ^2CH	7·52
				ζ^3CH	7·20
				η^2CH	7·29

*αCH of His and Trp were not observed in D_2O-H_2O because of the water resonance.

D_2O. A simple inspection of the various NOE data immediately indicated that the conformation of the peptide differed in organic and aqueous solution, as would be expected. Inter-residue NOEs spanning four or more amino acids were seen more commonly in d_6-DMSO, suggesting a well defined turn in the peptide backbone (Figure 1A), whereas in D_2O-H_2O the evidence indicated a close proximity between the disulphide bridge and Ile^6-Trp^7 and a well defined turn over the His^2-Leu^3-Asp^4 residues (Figure 1B). In both solvents Cys^1 to Cys^5 NOEs were found as a result of the cyclization.

ϕ Angles for the residues Cys^1, His^2, Ile^6 and Trp^7 in D_2O-H_2O were calculated to be $-170°$, $-133°$, $-146°$ and $-155°$, respectively. Unfortunately only the Asp ϕ angle could be determined with confidence from the 1-D ^1H NMR spectra for the peptide dissolved in d_6-DMSO; this was calculated as $-166°$. For the peptide dissolved in D_2O the side-chains of Cys^1 and Cys^5, His^2 and Trp^7 were determined to lie in a *trans* position (χ_1 angles of 180°) with the side-chain of Asp^4 shown to be disordered having $^{\alpha\beta}J_{Hz}$ of 6Hz and 8Hz.

Molecular modelling

The conformations of the peptide in D_2O-H_2O and d_6-DMSO were modelled using constrained molecular dynamics, incorporating the NMR-derived distance constraints and torsion angles. Distance violations calculated during the 15ps of MD at

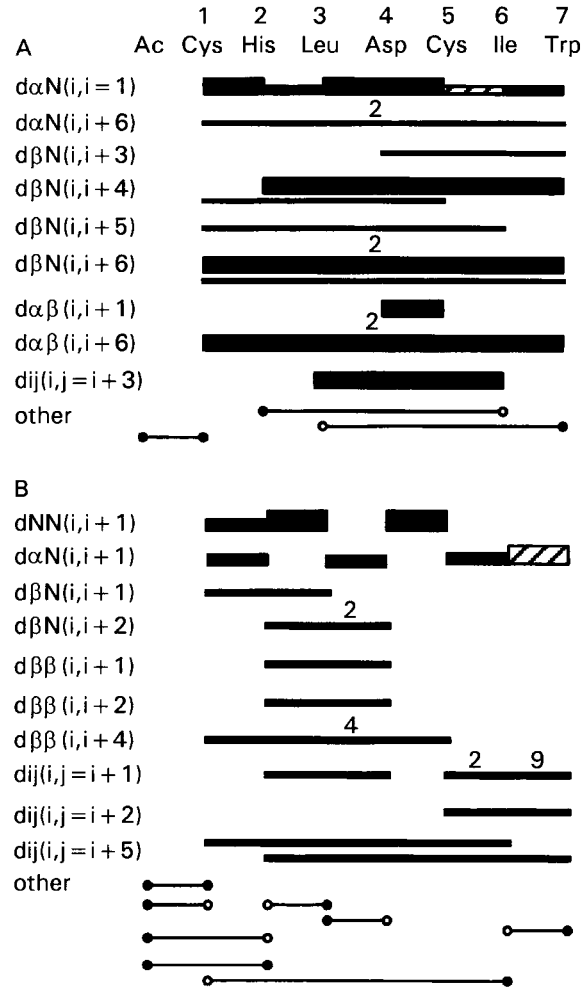

Figure 1. Summary of the inter-residue connectivities observed for the cyclic peptide dissolved in d_6-DMSO (A) and D_2O-H_2O (B). The solid bars represent the NOE (nuclear Overhauser effect) connectivity, the heights of which are proportional to the NOE intensity, this being classified as strong, medium or weak. The hatched bar indicates an NOE connectivity which could not be assigned unambiguously because of chemical-shift degeneracy. Where a particular NOE occurs more than once the number of occurrences is given above the bar. d_{ij} represents NOE connectivities between side-chain protons on residues i and j. NOE connectivities between main-chain and side-chain protons are represented by filled and empty circles, respectively.

750K were seen to remain within 1·0Å and torsion angles within ±30° of the applied limits. After cooling to 300K, the majority of the constrained parameters were still in good agreement with the target values. Although the extent of violation increased during the unconstrained energy minimization, the major deviations from target values were confined to interactions involving side-chain rather than main-chain atoms.

Of the 330 energy-minimized structures generated, conformers were selected which best represented the observed 2-D ^1H NMR data, giving 22 conformers from the D_2O-H_2O data set and 27

from the d_6-DMSO data set. Both groups of structures could be divided into more than one family on the basis of their backbone conformation, the group modelled on the basis of the D_2O-H_2O data showing the greatest variation, possibly because of the smaller number of intrachain long-range NOEs (Figure 2). Conformational differences were less evident when comparing the peptide backbone over the residues His-Leu-Asp. Indeed the conformers modelled on the basis of the d_6-DMSO and D_2O-H_2O data are very much the same over this region. This similarity arises presumably because these residues are cyclized by the disulphide bridge, and in consequence have a smaller amount of conformational variability than the C-terminal Ile and Trp residues.

Superpositions were made on the corresponding main-chain atoms in the endothelin 1 X-ray structure with root-mean-square differences in co-ordinates of approximately 2·6 Å for structures modelled on the basis of the d_6-DMSO data, and 0·9–2·5 Å for structures modelled using the D_2O-H_2O data (Figure 3A). Using the structure which gave the best fit to the corresponding main-chain atoms in the endothelin 1 X-ray structure, a superposition was also made on to the main-chain atoms of the potent endothelin A-selective antagonist BQ-123. Because the amino acid sequences for the two peptides are dissimilar, the residues Leu^3-Asp-Cys-Ile-Trp^7 in the cyclic peptide were superposed on the residues DAsp-Pro-DVal-Leu-DTrp of BQ-123 and gave a good fit with a root-mean-square difference over the main-chain atom co-ordinates of 0·77 Å (Figure 3B). The two Trp indole rings were also seen to have a similar orientation and the D-Asp side-chain of BQ-123 was oriented in a manner which closely matched that of the C-terminal carboxyl group of the cyclic peptide.

Comparison of the hydrogen-bonding within the cyclic peptide structures modelled on the basis of NMR data acquired in d_6-DMSO showed interactions between the C-terminal carboxyl and the His^2 imidazole ring, with little involvement of the Asp^4 carboxyl. Structures modelled on the basis of NMR data acquired in D_2O-H_2O showed the C-terminal carboxyl again interacting with the His^2 imidazole ring and the Asp^4 carboxyl was seen to interact with the Ile^6 NH or the His^2 and Trp^7 side-chains.

Circular dichroism

CD spectra for the peptide in the peptide region showed minima at approximately 195–200 nm (Figure 4) which although not immediately characteristic of an α-helix are qualitatively similar to the CD spectra of endothelin 1 (Perkins et al 1990), which itself has two disulphide bridges and α-helical structure. The absence of a second minimum at 222 nm might be explained by the presence of a disulphide, which gives rise to a maximum at approximately 228 nm (Hider et al 1988).

Spectra in the disulphide–aromatic region followed during titration to increasing pH showed a

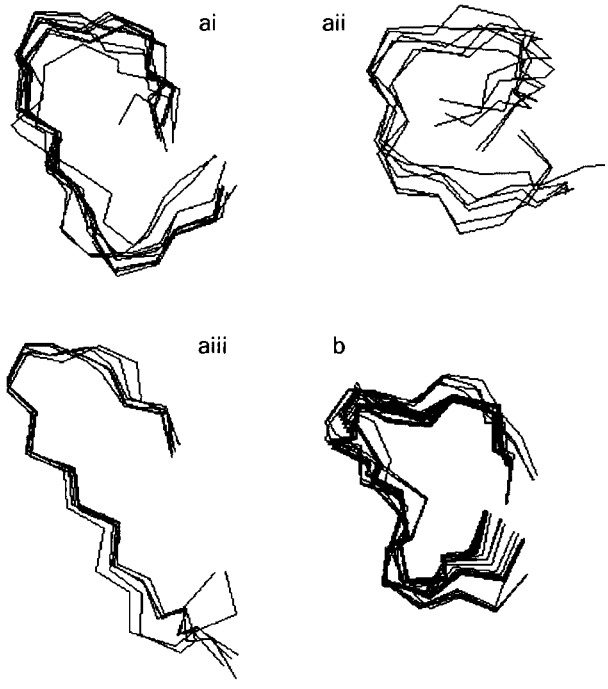

Figure 2. Superposition of low-energy cyclic peptide conformers, modelled on the basis of the NMR data acquired in D_2O-H_2O (A: 22 conformers, giving 3 distinct families, numbered i to iii) and d_6-DMSO (B: 27 conformers, 1 family), selected on the basis of their agreement with the applied experimental constraints.

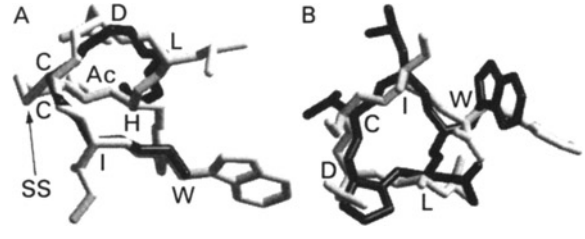

Figure 3. A. Superposition of the main-chain atoms for the cyclic peptide: Ac-cyclo(Cys-His-Leu-Asp-Cys)-Ile-Trp-OH (coloured grey) modelled from NMR data acquired in D_2O-H_2O and the corresponding atoms in the crystal structure of endothelin 1 (coloured black). For clarity, the side-chains are shown only for the cyclic peptide with amino acids labelled using single-letter amino acid codes (Ac, acetate; SS, disulphide bridge). The root-mean-square difference in co-ordinates over the main-chain atoms is 0·9 Å. B. Superposition of the main-chain atoms of the residues Leu^3-Asp-Cys-Ile-Trp^7 of the cyclic peptide in Figure 3A (coloured grey, with amino acids labelled using single-letter amino acid codes) and the corresponding atoms of the residues DAsp-Pro-DVal-Leu-DTrp of BQ-123 (coloured black). The root-mean-square difference in co-ordinates over the main-chain atoms is 0·77 Å.

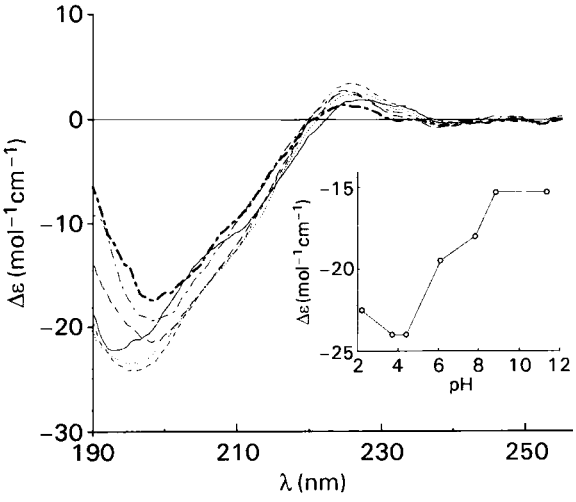

Figure 4. CD spectra recorded as a function of pH in the peptide region for the cyclic peptide dissolved in H_2O: ——, pH 2·2; . . . . . , pH 3·7; — — —, pH 4·4; - - - , pH 6·1; - · - · , pH 7·8; — · — , pH 11·3. The insert is a pH titration curve for the peptide backbone calculated at approximately 195 nm.

progression from negative to positive ellipticity over the range 240–280 nm, which is consistent with a change in handedness of the disulphide (Figure 5) (Woody 1995). This change was most noticeable at low pH, with little change above pH 7·8, the calculated titration curve suggesting an associated de-ionization of a carboxyl group (Figure 5, insert). For the spectra in the peptide region however, the same titration showed a more pronounced change towards neutral and basic pH, with the mimima moving from 195 to 200 nm (Figure 4) and the titration curve suggesting ionization of the His imidazole ring (Figure 4, insert). By comparison with these spectra, those recorded for the peptide dissolved in saturated sodium lauryl sulphate and in trifluoroethanol showed the disulphide–aromatic region to be qualitatively similar to that seen at high pH, with a shift in the peptide-region minimum to 205 nm (data not shown).

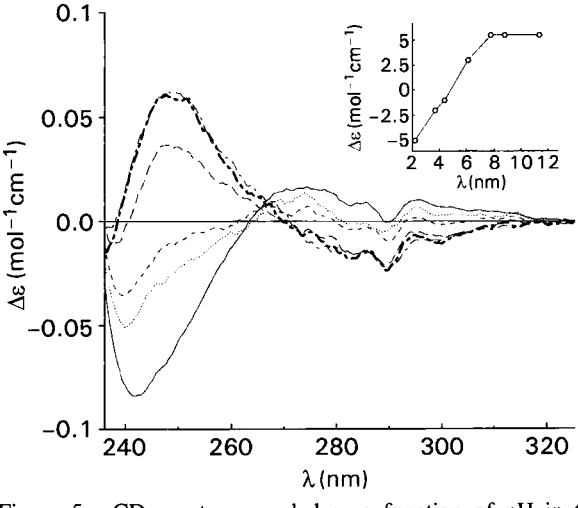

Figure 5. CD spectra recorded as a function of pH in the disulphide-aromatic region for the cyclic peptide dissolved in H_2O: ——, pH 2·2; · · · · · , pH 3·7; - - - -, pH 4·4; - - - , pH 6·1; — · — , pH 7·8; - - - , pH 11·3. The insert is a pH titration curve for the disulphide-aromatic region calculated at approximately 250 nm.

Pharmacology

The synthesized peptide did not have antagonist activity against endothelin-induced contraction of either rabbit aorta or bronchus at test concentrations of 15 μM (n = 4). A small upward shift to the aortal dose–response was seen, however, and further investigations for agonist activity showed that the peptide elicited weak contraction of the aorta at a concentration of 100 μM (data not shown).

Discussion

The differences seen in the conformers modelled from NMR data acquired in D_2O–H_2O and d_6-DMSO generally arise from differences in orientation of the Ile^6-Trp^7 dipeptide. Hydrophobic interactions might account for the tendency of the Ile^6 and Trp^7 side-chains to turn towards the disulphide (Andersen et al 1995) but the conformational differences seem more likely to arise from the distinct hydrogen-bonding patterns. In particular, the Asp^4 carboxyl was most notably involved in hydrogen-bonding only in structures modelled from the D_2O–H_2O data and its role in determining the conformation of the peptide main chain is consistent with the pH-dependent CD changes seen in the disulphide-aromatic region.

The cyclized peptide seems to have lost all pharmacological activity at the endothelin B receptor, even though its sequence is essentially identical to that of the endothelin 1 C-terminal hexapeptide. The substitution of Ile^{19} for Cys is not expected to prohibit recognition of the cyclic peptide by the endothelin A and endothelin B receptors because substitutions by Ala and Val at this position yield antagonists with full binding affinity (Cody et al 1995). This loss of activity is therefore thought to be because of the inability of the cyclic peptide to access the endothelin B receptor binding site in the manner achieved by the native endothelin hexapeptide and other linear peptide analogues.

Rather surprisingly, the cyclic peptide had no antagonist activity at the endothelin A receptor; this would be reasonably expected on the basis that a close match is seen between the endothelin A antagonist BQ-123 and the residues Leu^3-Asp-Cys-Ile-Trp^7 of the cyclic peptide (Figure 3B). It has been suggested that BQ-123 binds to a region of the

endothelin A receptor which is otherwise occupied by the endothelin C-terminal hexapeptide because the side-chains of the Asp^{18} and Trp^{21} residues in the endothelin crystal structure superpose on the corresponding side-chains of BQ-123 (Peishoff et al 1995). The results presented here indicate that the apparent mimicry of BQ-123 for the endothelin C-terminal region might not be entirely correct and that its mimicry of other regions should not be discounted.

In hindsight, it would clearly have been preferable to use endothelin receptor binding assays to determine whether the hexapeptide had any affinity at endothelin A or endothelin B receptors. On the basis of our observations above, however, we tentatively propose that the conformational flexibility of a peptide ligand might govern, in part, its selectivity for the endothelin A receptor as opposed to endothelin B receptor. Specifically, we propose that a large amount of conformational flexibility, as would be expected for the linear endothelin C-terminal analogues, makes binding at the endothelin A receptor entropically unfavourable but facilitates access to the endothelin B receptor binding site. In contrast, with a highly constrained peptide such as BQ-123 there is no binding at the endothelin B receptor but antagonist activity is observed at the endothelin A receptor. Because the cyclic peptide studied here lies between these two extremes, it consequently retains some residual agonist activity at the endothelin A receptor, but is too constrained to access the endothelin B receptor binding site. Furthermore, assuming that the cyclic peptide designed here does provide a good fit to the intended α-helical motif in endothelin 1 (at least with the peptide in free solution, Figure 3A) then it is unlikely that the conformation of the C-terminal tail seen in the crystal structure of endothelin gives a complete picture of the pharmacophore relevant to the endothelin B receptor.

Acknowledgements

NMR experiments were performed by Mrs J. Hawkes at the University of London Intercollegiate Research Service, and CD experiments were performed at the Optical and Spectroscopic Unit at King's College London. This work was supported by a grant from the Wellcome Trust, Euston Road, London.

References

Andersen, N. H., Chen, C. P., Lee, G. M. (1995) The endothelin C-terminal signal fragment-determinants of the conformational equilibrium in situ and detached. Protein Peptide Lett. 1: 215–222

Barnes, P. J. (1994) Endothelins and pulmonary diseases. J. Appl. Physiol. 77: 1051–1059

Barsukov, I. L., Lian, L.-Y. (1993) NMR of macromolecules: a practical approach. In: Roberts, G. C. K. (ed.), IRL Press, Oxford, pp 323–327

Clozel, M., Watanabe, H. (1993) BQ-123, a peptide endothelin A receptor antagonist, prevents the early cerebral vasospasm following subarachnoid hemorrhage after intracisternal but not intravenous injection. Life Sci. 52: 825–834

Cody, W. L., He, J. X., DePue, P. L., Waite, L. A., Leonard, D. M., Sefler, A. M., Kaltenbronn, J. S., Haleen, S. J., Walker, D. M., Flynn, M. A., Welch, K. M., Reynolds, E. E., Doherty, A. M. (1995) Structure–activity relationships of the potent combined endothelin-A/endothelin-B receptor antagonist Ac-DDip[16]-Leu-Asp-Ile-Ile-Trp[21]: Development of endothelin-B receptor-selective antagonists. J. Med. Chem. 38: 2809–2819

Coles, M., Sowemimo, V., Scanlon, D., Munro, S. L. A., Craik, D. J. (1993) A conformational study by ^{1}H NMR of a cyclic pentapeptide antagonist of endothelin. J. Med. Chem. 36: 2658–2665

Hider, R. C., Kupreyszweski, G., Rekowski, P., Lammek, B. (1988) Origin of the 225–230 nm circular dichroism band in proteins — its application to conformational analysis. Biophys. Chem. 31: 45–51

Ishikawa, K., Fukami, T., Nagase, T., Fujita, K., Hayama, T., Nijyama, K., Mase, T., Ihara, M., Yano, M. (1992) Cyclic pentapeptide endothelin antagonists with high endothelin A selectivity. Potency and solubility-enhancing modifications. J. Med. Chem. 35: 2139–2142

Janes, R. W., Peapus, D. H., Wallace, B. A. (1994) The crystal structure of human endothelin. Struct. Biol. 1: 311–319

Kurihara, Y., Kurihara, H., Suzuki, H., Kodama, T., Maemura, K., Nagai, R., Oda, H., Kuwaki, T., Cao, W.-H., Kamada, N., Jishage, K., Ouchi, Y., Azuma, S., Toyoda, Y., Ishikawa, T., Kumada, M., Yazaki, Y. (1994) Elevated blood pressure and craniofacial abnormalities in mice deficient in endothelin 1. Nature 368: 703–710

Maggi, C. A., Giuliana, S., Patacchini, R., Rovero, P., Giachetti, A., Meli, A. (1989) The activity of peptides of the endothelin family in various mammalian smooth muscle preparations. Eur. J. Pharmacol. 174: 23–31

Marrion, D., Wüthrich, K. (1983) Applications of phase sensitive two-dimensional correlated spectroscopy (COSY) for measurement of ^{1}H-^{1}H spin-spin coupling constants in proteins. Biochem. Biophys. Res. Commun. 113: 967–974

McLachlan, A. D. (1979) Gene duplication in the structural evolution of chymotrypsin. J. Mol. Biol. 128: 49–79

Mills, R. G., O'Donoghue, S. I., Smith, R., King, G. F. (1992) Solution structure of endothelin-3 determined using NMR spectroscopy. Biochemistry 31: 5640–5645

Mino, N., Kobayashi, M., Nakajima, A., Amano, H., Dhimamoto, K., Ishikawa, K., Watanabe, K., Nishikibe, M., Yano, M., Ikemoto, F. (1992) Protective effect of a selective endothelin receptor antagonist, BQ-123, in ischemic acute renal failure in rats. Eur. J. Pharmacol. 221: 77–83

Newby, D. E., Webb, D. J. (1996) Advances in clinical pharmacology and therapeutics—endothelin. Br. J. Hosp. Med. 56: 360–364

Peishoff, C. E., Janes, R. W., Wallace, B. A. (1995) Comparison of the structures of the endothelin A receptor antagonists BQ123 and *N*-methylleucine BQ123 with the crystal structure of the C-terminal tail of endothelin 1. FEBS Lett. 374: 379–383

Pelton, J. T. (1991) Fluorescence studies of endothelin 1. Neurochem. Int. 18: 485–489

Perkins, T. D. J., Barlow, D. J. (1990) RAMBLE: a conformational search program. J. Mol. Graph. 8: 156–162

Perkins, T. D. J., Hider, R. C., Barlow, D. J. (1990) Proposed solution structure of endothelin. Int. J. Peptide Protein Res. 36: 128–133

Saudek, V., Hoflack, J., Pelton, J. T. (1991) Solution conformation of endothelin 1 by ^{1}H NMR, CD, and molecular modelling. Int. J. Peptide Protein Res. 37: 174–179

Sutcliffe, M. J. (1993) NMR of macromolecules: a practical approach. In: Roberts, G. C. K. (ed.), IRL Press, Oxford, pp 359–387

Van der Walle, C. F., Bansal, S., Barlow, D. J. (1996) A cyclic hexapeptide mimic of the endothelin C-terminus. Pharm. Sci. 2: 59–63

Wallace, B. A., Janes, R. W. (1995) The crystal structure of human endothelin 1 and how it relates to receptor binding. J. Cardiovasc. Pharmacol. 26 (Suppl. 3): S250–S253

Weiner, S. J., Kollman, P. A., Nguyen, D. T., Case, D. A. (1986) An all-atom force-field for the simulation of proteins and nucleic acids. J. Comput. Chem. 7: 230–252

Woody, R. W. (1995) Circular dichroism. Methods Enzymol. 246: 34–71

Wüthrich, K. (1986) NMR of Proteins and Nucleic Acids. John Wiley & Sons, New York

Yanagisawa, M., Kurihara, H., Kimura, S., Tomobe, Y., Kobayashi, M., Mitsui, Y., Yazaki, Y., Goto, K., Masaki, T. (1988) A novel potent vasoconstrictor peptide produced by vascular endothelial cells. Nature 332: 411–415